NUMERICAL ASSESSMENT OF AN AIR-HEAT EXCHANGER CHANNEL WITH STAGGERED ATTACHED RECTANGULAR BAFFLES AND IN-LINE DETACHED SQUARE FINS

by

Redha REBHI[a,b], Hijaz AHMAD[c,d], Yun-Hui ZHAO[e*], Younes MENNI[f], and Giulio LORENZINI[g]

[a] Department of Mechanical Engineering, Faculty of Technology, University of Medea, Medea, Algeria
[b] LERM - Renewable Energy and Materials Laboratory, University of Medea, Medea, Algeria
[c] Operational Research Center in Healthcare, Near East University, Nicosia/Mersin, Turkey
[d] Section of Mathematics, International Telematic University Uninettuno, Roma, Italy
[e] School of Mathematics and Information Science, Henan Polytechnic University, Jiaozuo, China
[f] Department of Technology, University Center Salhi Ahmed Naama, Naama, Algeria
[g] Department of Industrial Engineering, University of Parma, Parma, Italy

Original scientific paper
https://doi.org/10.2298/TSCI23S1343R

The study's main objective is to assess a channel heat exchanger's thermal and hydraulic characteristics in the presence of turbulent air-flow at a fixed Reynolds number. Using two distinct versions of the obstacles in terms of their shape, fixation, and arrangement, the baffles and fins are implanted inside the channel. To convert a conventional flow path into a wave-shaped one, a first model contains rectangular baffles alternately distributed throughout the channel surfaces. According to the horizontal axis of the channel, between the edges of the baffles in the first type, the second model relates to square and in-line deflectors (fins). On each of the channel's solid bounds, the boundary criteria are specified. An k-ε turbulence model was used to build the mathematical model for flow and energy. As might be predicted, the pressure, velocity, and temperature fields exhibit the greatest fluctuations in the areas closest to the obstacles.

Key words*: staggered arrangement, in-line arrangement, attached baffles, detached fins, rectangular channel, air-flow turbulent, forced-convection*

Introduction

The heat exchanger is an essential component of many thermal processes such as heating, cooling, drying, *etc*. Improving its performance is the goal of many researchers. Its internal restructuring is among the most common methods, such as adding fins and ribs. The methodology used has shown an improvement in thermal and dynamic performance, for example, Rani *et al*. [1] conducted an experimental evaluation of the combined solar air heater with turbulators in the shape of hollow semicircular rings to determine its temperature distribution, heat transfer coefficients, and thermal efficiency. The results showed that the air temperature was lower than that of the rings and absorber, but higher than that of the glass. Additionally, the average air temperature rise in finned collectors changes by 14.08-22.78 °C, which is a significant change when compared to conventional solar collectors. On the absorption surface,

* Corresponding author, e-mail: zhaoyunhui2019@163.com

Promvonge and Skullong [2] investigated the hydraulic and thermal performance of a solar channel outfitted with a V-barbed vortex flow generator. The ideal parameters of the employed barriers and their correlations have been presented, along with experiments on the flow friction and heat transfer behaviors. El Habet *et al*. [3] carried out an experiment with an aspect ratio of roughly 3:1 to document the impact of barriers on the flow structure and heat distribution within a rectangular channel. These barriers are present intermittently and steadily on the lower and upper surfaces. Additionally, a homogeneous heat flow has been applied to both surfaces, and the side surfaces have been insulated. In their computational analysis, Bhattacharyya *et al*. [4] relied on the influence of an external magnetic field to remove the excessive heat flow at low Reynolds values. This is accomplished by using magnetic force to produce vortices with the intention of enhancing heat transmission. A 2-D heated channel was employed with a nanomagnetic Fe_3O_4 aqueous fluid under the impact of low Reynolds number. Yadav *et al*. [5] presented a detailed study reviewing the performance of solar panel heaters. The effectiveness of using synthetic roughness in improving thermal performance for a compact design of the device has been discussed.

Mohit *et al.* [6] ran a numerical simulation based on changing the height of pin fins (0.2-1.0 mm) inside a micro-channel that had a constant heat flow at its bottom part while having a varied hydraulic flow due to changes in the Reynolds number (200-1000). The results showed that improving the Reynolds number and raising the fin height increased heat transmission. Using six distinct barrier models, Boonloi *et al*. [7] made a detailed evaluation of the thermal and flow performance of a square-shaped channel. In their investigation, laminar flow processes were established for various Reynolds number values (100-2000) in the presence of various factors, including blockage rates, barrier size and their different shapes, as well as different flow directions for enhanced Nusselt number. Sharma *et al*. [8] carried out a computational study using the hybrid Taguchi-TOPSIS method that was primarily focused on optimizing the discrete-V-down -structural barrier's design in order to improve the heat transfer of a solar collector channel. Their research demonstrated an improvement and detailed understanding of how these obstacles affect the efficiency of air current-based solar collector ducting. Kumar *et al*. [9] investigated the combined effect of intermittent circular roughness and jet impingement to assess the effectiveness of air-based solar heaters. According to estimates, the rough heater case's heat transmission and friction values are, respectively 7.61 and 6.48 times higher than those of the smooth channel case. In contrast, the enhanced solar heater had a thermal performance of around 4.1. In an air solar heater, Singh *et al*. [10] compared several roughness results, *i.e*., boot and reverse boot. The outcomes are discovered with the aid of CFD simulations for several boot-shaped rib configurations on solar air heaters. In order to improve the heat performance of the air heater, the combined roughness of the boot and reverse boot form is examined for various geometrical parameters.

Chand *et al*. [11] introduced barriers with apertures where the thermal performance was assessed, resulting in a new type of solar heaters based on air-flows. In order to guide the air-flow and quicken the rate of heat transfer, the study experimented with fastening the louvered barriers to the lower of the absorbent plate. The findings showed that the thermal efficiency rises with the flow rate; at a rate of mass-flow of 0.0158 kg/s and 0.007 kg/s, maximum thermal-efficiency and outlet-temperature were obtained, respectively, at 70% and 58.66 °C for a distance of separation of 2 cm.

Three different types of trapezoidal turbulators were created in Li *et al*. [12] investigation using the corrugated triangular-shaped configuration. By using numerical simulations,

it was determined how the apex angle and turbulator location affected the flow characteristics and heat transfer in the corrugated triangular flow duct fitted by trapezoidal-shaped turbulators. The friction values of flow ducts fitted by an apex angle of 60° or 90° were near in order and higher than those of 120° for various vertex values. The heat transfer rates showed the same trend. The flow duct has the highest values for friction, heat transfer, and performance when the turbulators are in the middle of the top part of the duct. In a conduit that was partially heated by constant heat transfer, Ismael [13] looked at the interplay between fluid-flow structure and forced-convection. The compliant segment was restricted by two models, upstream and downstream barriers working as turbulators. It is discovered that the pressure loss rises by 210% while the rate of heat transfer for a given compatible baffled conduit case increases by 94% when compared to the non-finned conduit case at Re = 250. Thermo-hydraulic research revealed that the upstream and downstream barriers' lengths should be 0.6 and 0.2 times the conduit height, respectively, to get the greatest performance at Cauchy number 10-7.

In a numerical study conducted by Kitayama *et al*. [14], the baffle structure was reinforced for irregular flow and pressure drop. They observed from the computational results that the ideal baffle situation, when compared to the traditional structure, may greatly enhance the flow irregularity and pressure loss. Through design optimization, improvements in pressure loss and flow irregularity of around 23% and 34%, respectively, over the standard configuration were made. To determine the best thermal performance for Reynolds numbers ranging from 4400- 20400 in a rectangular channel, Sriromreun *et al*. [15] looked at the impacts of the Z-barrier size and separation length. When operating under similar conditions, it was discovered that the in-phase 45° Z-type barriers had significantly greater heat transfers, friction coefficients, and thermal intensification factors than the out-phase 45° Z-type barriers produced. While the lower separation length produced the higher thermohydraulic performance than the wider one, the in-phase 45° Z-type barrier with the bigger height offered more heat transfer and friction loss than the one with the smaller height.

In the current study, a 2-D simulation of a rectangular channel heat exchanger containing two distinct models of obstacles, namely, rectangular baffles connected to the channel walls in an overlapping manner that allows changing the flow shape from regular to wavy, while the second model includes detached square-shaped deflectors, in a horizontal in-line arrangement in the middle of the channel, precisely between the upper edges of the obstacles of the first model. The study allowed for the simultaneous employment of attached baffles and detached deflectors on the one hand, and the utilization of two distinct obstacle arrangements, overlapping and sequential, as well as the combination of two different rectangular and square obstacle shapes, on the other hand. Both the flow parameters and the channel's overall temperature distribution are assessed.

Modelling and simulation

The 2-D simulation of a heat exchanger channel as designed in fig. 1. Turbulent airflow traverses the channel, from left to right, according to a constant value of the Reynolds number. In order to improve the hydraulic and thermal structure of the channel, a set of barriers are inserted across the flow. There are two distinct classes of these barriers that were designed in this study. The first set consists of two rectangular baffles that are alternately mounted vertically on the canal's two surfaces [16]. While the second set included four horizontally sequential square fins, located in the central part of the channel, between the left and right top edges of the first and second attached baffles, respectively.

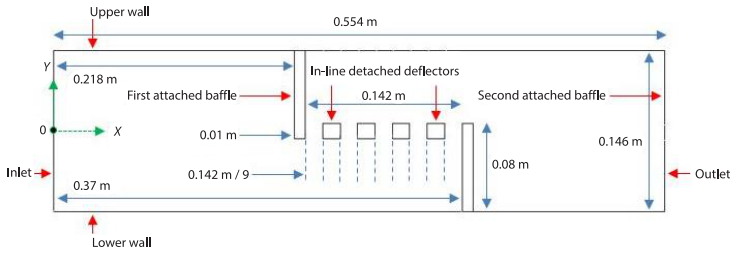

Figure 1. Model of the baffled channel with in-line detached square-fins under study

Demartini *et al*. [16] numerical and experimental study served as the foundation for the current design. In their research, the hydraulic performance of turbulent air-flow across two staggered attached baffles (the first set of barriers) was assessed. With the addition of in-line detached square-shaped deflectors (the second set of barriers), their channel structure is enhanced in the current study for a more turbulent structure and better fluid mixing. All dimensions are shown in fig. 1, which were determined based on the same previous literature study [16], except for the dimensions of the second set of barriers (fins) that were designed in the current study.

Boundary conditions must be provided for all surfaces in order to model the proposed construction, fig. 2. Taking a look at the intake channel first, which has a constant velocity (U_{in} = 7.8 m/s) and a constant Reynolds number of $8.73 \cdot 10^4$ [16]. A constant temperature of 375 K [17] is applied to the top and lower portions of the channel, which are located behind and in front of the upper and lower attached baffled, respectively. The rest of the areas are thermally insulated including the attached and detached barriers. At last, the channel's outlet's atmospheric pressure is established.

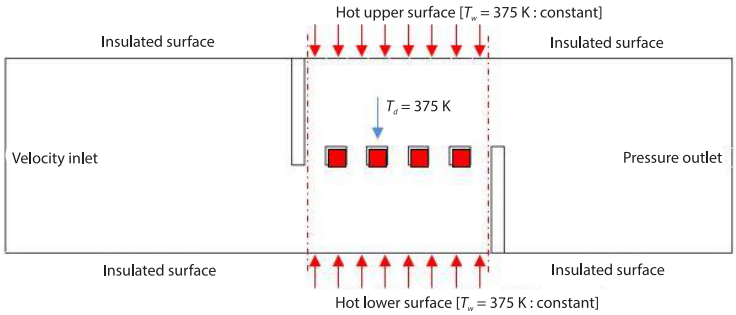

Figure 2. Boundary conditions

In the present study, an incompressible turbulent Newtonian current flow (air) within a baffled channel whose boundary conditions are defined previously. The conservation equation of a scalar variable ϕ can be expressed in its 2-D form [18]:

$$\frac{\partial}{\partial x}(\rho u\varphi)+\frac{\partial}{\partial y}(\rho v\varphi)=\frac{\partial}{\partial x}\left[\Gamma_\varphi\frac{\partial\varphi}{\partial x}\right]+\frac{\partial}{\partial y}\left[\Gamma_\varphi\frac{\partial\varphi}{\partial y}\right]+S_\varphi \tag{1}$$

where ϕ is the variable that serves to represent quantities such as the velocity components u and v, k – the turbulent kinetic energy, ε – the rate of turbulent energy dissipation, and T – the temperature. However, the coefficient of diffusion Γ_ϕ and the source term S_ϕ have specific values for the different conservation equations for the case of the standard k-ε turbulence model. More details are found in [18].

The mesh is refined at all solid boundary points and is structurally quadrilateral non-uniform in 2-D. The heat transfer and fluid-flow are modeled using the finite volume approach [19], the SIMPLE algorithm [19], the QUICK scheme [20], the *k*-model, and the FLUENT program is utilized for this analysis.

To examine the efficiency and reliability of the numerical code, a coefficient of pressure calculated. This coefficient of pressure was governed by the flow velocity U_{in} = 7.8 m/s, or Re = 8.73 · 10^4, and the rate of inlet turbulence intensity is 2% [16]. The standard *k*-*ε* turbulence model was applied [21]. The obtained numerical results were compared with the experimental and numerical data of Demartini *et al*. [16]. The computational results presented in fig. 3 are in agreement with the experimental and numerical results.

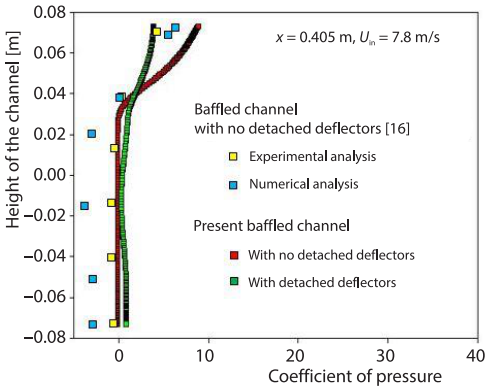

Figure 3. Model of the validation

Results and discussion

The streamlines for Re = 8.73 · 10^4 are shown in fig. 4. When the first attached baffle is present, leading and upstroke vortices start to form, and the flow passes both the first attached and detached deflectors. The flow stagnates at the windward surface of the obstacle as the vortices shrink and approaching the second attached baffle. At the frontal base of the second attached baffle, a little vortex is created by some fluid-flowing toward the bottom. The fluid-flowing towards the roof separates at the windward edge of the roof forming a small re-circulation bubble at the top of the second attached baffle. At the leading edge, the flow separating creates wake of highly recirculating flow, behind the obstacle, that is dominated by an arch-shaped vortex in the wake region.

The Dynamic pressure is the flow of momentum per unit volume (the kinetic energy density) is shown in fig. 5. The figure shows that dynamic pressure increases dramatically in narrow flow regions, and decreases in the container regions of the recycling cells.

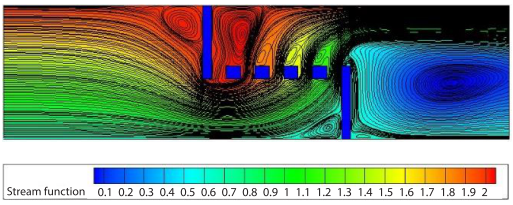

Figure 4. Streamlines

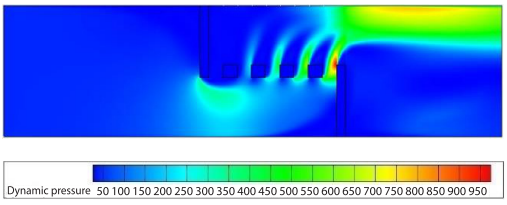

Figure 5. Field of dynamic-pressure

The average speed is the total distance traveled during a time interval, divided by that time interval. Figure 6 shows that the vortex is always generated upstream of the first attached baffle. It is also observed that, the average speed increases continuously because the flow passes the datached deflectors. The influence of the edge downstream of the obstacle is not limited to the re-circulation zone, but it modifies the behavior of the fluid even upstream of this edge. Its is extended to the vicinity of this obstacle (attached baffle or detached deflectors).

Figure 7 represents the variation of the axial velocity for Re = 8.73 · 10^4. It is shown that the flow is actually accelerated when facing the obstacle. The axial speed is important up-

stream of second attached baffle, because the perfect straightening of the flow. In the detached deflectors the speed is disturbed. On the other hand, in the upstream of the second attached baffle the speed is alternating because the vortex generated.

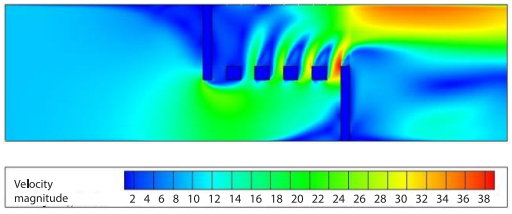

Figure 6. Field of velocity-magnitude

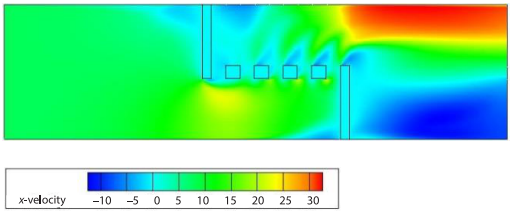

Figure 7. Field of axial velocity

Figures 8 and 9 shows the profiles of the *X*-velocity component at different sections: under, above and downstream the attached baffles. It can show that, the profile is well correctly predicted. The regions in which the turbulence model starts fail to estimate the correct velocity that corresponds to the onset of the recycling vortex formed at the forward base of the attached baffle. The rapid change in the high pressure gradient, caused by the stagnation point, prevents the flow field from being adequately captured, in this region. Above the attached first baffle, the *k*-turbulence model more accurately predicts the *X*-velocity profile especially near the wall where small-volume bubble separation occurs. Just downstream of the obstacle, a slight deviation was observed at about the medium-height attached baffle.

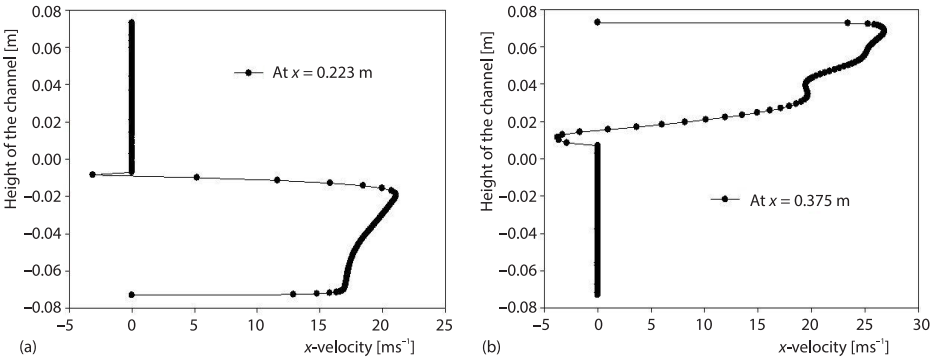

Figure 8. The *X*-profiles of the velocity; (a) under and (b) above the 1st and the 2nd baffles, respectively

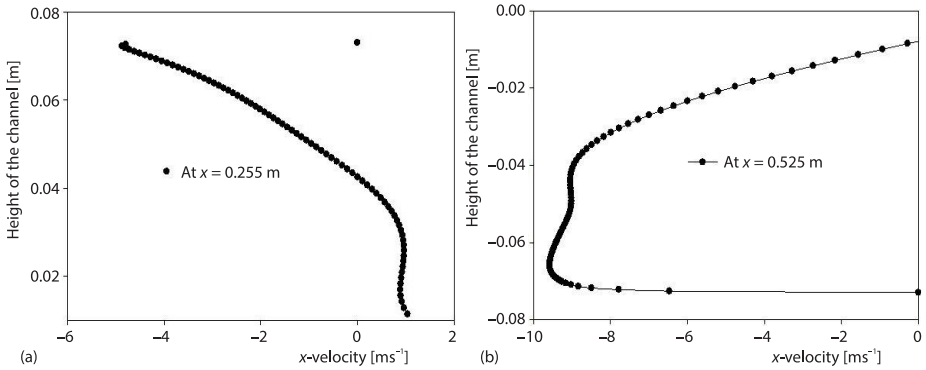

Figure 9. The *X*-profiles of the velocity downstream of (a) the 1st and (b) the 2nd baffles

Figure 10 represents the variance of vertical velocity (Y-velocity). The meteor's vertical velocity is nearly zero, except that the walls face the flow, but the signal depends on the direction of the flow. Velocity is important upstream of the 2nd attached baffle due to the sudden drop in the channel section.

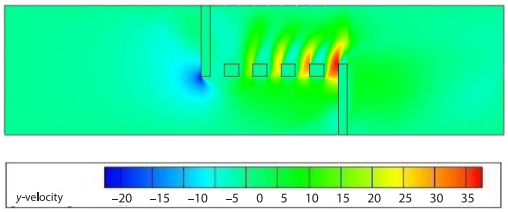

Figure 10. Field of transversal velocity

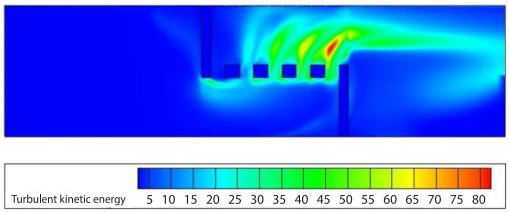

Figure 11. Field of turb-kinetic-energy

In figs. 11-13 representing the difference in the turbulent kinetic energy field, the turbulent dissipation rate, the turbulence intensity and the turbulent viscosity, respectively, for $Re = 8.73 \cdot 10^4$. At the inlet, the turbulent kinetic energy is simply dissipated by the viscosity effect, so there is a balance between heat flow and viscous rate of dissipation in the transfer equation for k, where there is neither a production mechanism (no velocity gradient) nor a diffusion mechanism (no k gradient). In general, in terms of the universal qualitative form, the turbulent power is restored and increased for each detached deflector.

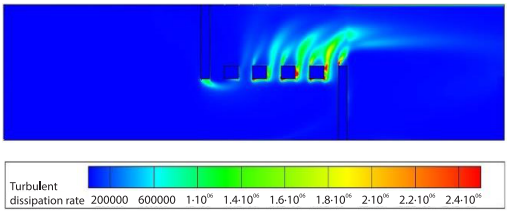

Figure 12. Field of turb-diss-energy

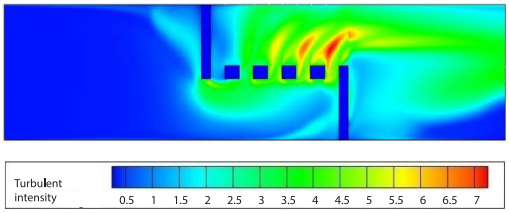

Figure 13. Field of turb-intensity

Figure 14 shows the temperature distribution of the detached deflectors and the hot upper and lower surfaces of the duct. It is noted that in the case downstream of the first detached obstacle, the contact between the cold zone and the attached baffle is large, because the re-circulation of the flow is important. We also observed that downstream of the second detached obstacle, the contact between cold air and the lower wall of the duct is poor, due to the presence of a large re-circulation area that acts as a barrier to the temperature distribution.

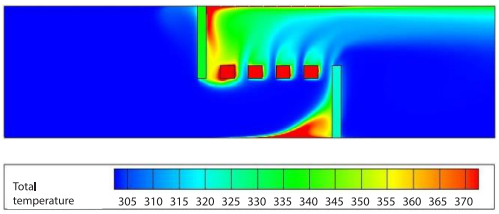

Figure 14. Field of temperature, $Re = 8.73 \cdot 10^4$

Conclusion

Principal findings include are as follows.

- A strongly recirculating flow wake is produced behind the obstruction at the leading edge of the flow separation, and the wake region is dominated by an arch-shaped vortex.
- In the recycling cells' container sections, the dynamic pressure falls, but it rises rapidly in the narrow flow regions.

- The edge downstream of the obstruction has an impact on the fluid behavior upstream as well as downstream, not just in the re-circulation zone.
- Upstream of the second attached baffle, where the flow is perfectly straightened, the axial speed is crucial. The speed is erratic in the disconnected deflectors.
- There is a balance between heat flow and viscous rate of dissipation in the transfer equation for k because there is neither a production mechanism (no velocity gradient) nor a diffusion mechanism at the intake where the turbulent kinetic energy is simply wasted by the viscosity effect (no k gradient).
- In general, for each disconnected deflector, the turbulent power is augmented and restored in terms of the universal qualitative form.
- Because the re-circulation of the flow is crucial, it should be noted that in the scenario downstream of the first detached obstacle, there is significant contact between the cold zone and the attached baffle.

References

[1] Rani, P., Tripathy, P. P., Experimental Investigation on Heat Transfer Performance of Solar Collector with Baffles and Semicircular Loops Fins Under Varied Air Mass-flow Rates, International Journal of Thermal Sciences, *178* (2022), 107597
[2] Promvonge, P., Skullong, S., Thermal-Hydraulic Performance Enhancement of Solar Receiver Channel by Flapped V-Baffles, *Chemical Engineering Research and Design*, *182* (2022), June, pp. 87-97
[3] El Habet, M. A., *et al*., The Effect of Using Staggered and Partially Tilted Perforated Baffles on Heat Transfer and Flow Characteristics in A Rectangular Channel, *International Journal of Thermal Sciences*, *174* (2022), 107422
[4] Bhattacharyya, S., *et al*., Thermo-Hydraulic Performance of Magnetic Baffles for Removal of Concentrated Heat Fluxes in a Heated Mini Channel, *Applied Thermal Engineering*, *216* (2022), 118992
[5] Yadav, A. S., *et al.*, Performance Enhancement of Solar Air Heater by Attaching Artificial Rib Roughness on the Absorber Plate, *Materials Today, Proceedings*, *63* (2022), 7, pp. 706-717
[6] Mohit, M. K., Gupta, R., Numerical Investigation of the Performance of Rectangular Micro-Channel Equipped with Micro-Pin-Fin, *Case Studies in Thermal Engineering*, *32* (2022), 101884
[7] Boonloi, A., Jedsadaratanachai, W., The CFD Analysis on Heat Transfer Characteristics and Fluid-Flow Structure in a Square Duct with Modified Wavy Baffles, *Case Studies in Thermal Engineering*, *29* (2022), 101660
[8] Sharma, A., *et al*., Experimental Investigation and Optimization of Potential Parameters of Discrete V Down Baffled Solar Thermal Collector Using Hybrid Taguchi-TOPSIS Method, *Applied Thermal Engineering*, *209* (2022), 118250
[9] Kumar, R., *et al*., Thermo-Hydraulic Efficiency and Correlation Development of an Indoor Designed Jet Impingement Solar Thermal Collector Roughened with Discrete Multi-Arc Ribs, *Renewable Energy*, *189* (2022), Apr., pp. 1259-1277
[10] Singh, H., *et al.*, The CFD Simulation of Thermal Hydraulic Performance of Rectangular Solar Air Heater with Combination of Boot Rib Roughness, *Materials Today, Proceedings*, *65* (2022), 8, pp. 3860-3865
[11] Chand, S., *et al.*, Thermal Performance Enhancement of Solar Air Heater Using Louvered Fins Collector, *Solar Energy*, *239* (2022), June, pp. 10-24
[12] Li, Z. X., *et al.*, The Effect of Trapezoidal Baffles on Heat and Flow Characteristics of a Cross-Corrugated Triangular Duct, *Case Studies in Thermal Engineering*, *33* (2022), 101903
[13] Ismael, M. A., Forced Convection in Partially Compliant Channel with Two Alternated Baffles, *International Journal of Heat and Mass Transfer*, *142* (2022), 118455
[14] Kitayama, S., *et al.*, Numerical Optimization of Baffle Configuration in Header of Heat Exchanger Using Sequential Approximate Optimization, *Simulation Modelling Practice and Theory*, *115* (2022), 102429
[15] Sriromreun, P., *et al.*, Experimental and Numerical Study on Heat Transfer Enhancement in a Channel with Z-Shaped Baffles, *International Communications in Heat and Mass Transfer*, *39* (2012), 7, pp. 945-952
[16] Demartini, L. C., *et al.*, Numeric and Experimental Analysis of The Turbulent Flow Through a Channel with Baffle Plates, *Journal of the Brazilian Society of Mechanical Sciences and Engineering*, *26* (2004), 2, pp. 153-159

[17] Siddiqui, M. K., Heat Transfer Augmentation in a Heat Exchanger Tube Using a Baffle, *International Journal of Heat and Fluid-flow*, *28* (2007), 2, pp. 318-328
[18] Yang, Y. T., Hwang, C. Z., Calculation of Turbulent Flow and Heat Transfer in a Porous-Baffled Channel, *International Journal of Heat and Mass Transfer*, *46* (2003), 5, pp. 771-780
[19] Patankar, S.V., *Numerical Heat Transfer and Fluid-flow*, McGraw-Hill, New York, USA, 1980
[20] Leonard, B. P., Mokhtari, S., Ultra-Sharp Non-Oscillatory Convection Schemes for High-Speed Steady Multidimensional Flow, NASA TM 1-2568, NASA Lewis Research Center, Cleveland, O., USA, 1990
[21] Launder, B. E., Spalding, D. B., The Numerical Computation of Turbulent Flow, *Computer Methods in Applied Mechanics and Engineering*, *3* (1974), 2, pp. 269-289

Paper submitted: February 23, 2022
Paper revised: March 14, 2022
Paper accepted: March 27, 2022